Journal of Organometallic Chemistry 897 (2019) 50–56

Contents lists available at ScienceDirect

Journal of Organometallic Chemistry

journal homepage: www.elsevier.com/locate/jorganchem

Rhodium-catalyzed formation of silylcarbamates from the reaction of secondary amines with CO_2 and hydrosilanes

Jefferson Guzmán, Adrián Torguet, Pilar García-Orduña, Fernando J. Lahoz, Luis A. Oro, Francisco J. Fernández-Alvarez*

Departamento de Química Inorgánica-Instituto de Síntesis Química y Catálisis Homogénea (ISQCH), Universidad de Zaragoza – CSIC, Facultad de Ciencias, 50009, Zaragoza, Spain

ARTICLE INFO

Article history:
Received 29 April 2019
Received in revised form
5 June 2019
Accepted 12 June 2019
Available online 20 June 2019

Keywords:
CO_2-Reduction
Rhodium
Homogenous catalysis
Silylcarbamates
Hydrosilylation

ABSTRACT

The reaction of (4-methyl-pyridine-2-iloxy)dimethylsilane (NSi^{Me}–H, **1**) with $[RhCl(coe)_2]_2$ gives the rhodium(III) complex $[Rh(Cl)(\kappa^2\text{-}NSi^{Me})_2]$ (**2**), which reacts with a stoichiometric amount of $AgCF_3CO_2$ to afford $[Rh(\kappa^2\text{-}CF_3CO_2)(\kappa^2\text{-}NSi^{Me})_2]$ (**3**). Complexes **2** and **3** have been fully characterized by elemental analysis and NMR spectroscopy. The solid-state structure of **3** has been confirmed by X-ray diffraction analysis. Moreover, the activity of complex **3** as catalyst for the reaction of secondary amines with CO_2 (3 bar) and hydrosilanes has been studied. The outcomes of these catalytic studies show that under these conditions complex **3** promotes the selective formation of silylcarbamates.

1. Introduction

Pyridine-2-iloxy-silyl based anions could be considered promising ligands due to their electronic and steric versatility, which includes their potential as monoanionic bidentate (κ^2-NSi), tridentate (κ^3-N_2Si) or tetradentate (κ^4-N_3Si) ligands [1,2], In addition, their steric hindrance, sigma donor ability of the nitrogen atom(s) and *trans* influence of the silyl group could be easily tuned by choosing the proper substituents at the pyridinic ring(s) and/or the silicon atom (Fig. 1). However, this type of ligands presents the disadvantage that the functionalized silanes used as precursors are very reactive and hydrolyze easily in the presence of traces of moisture. This may be one of the reasons why the transition metal coordination chemistry of this type of ligands has been scarcely explored so far [1,2].

In this context, it is worth mentioning that in recent years we have demonstrated that rhodium and iridium complexes with pyridine-2-iloxy-silyl based ligands are excellent catalysts for hydrosilylation and/or silylation processes [2]. For example, iridium-(*fac*-κ^3-N_2Si) complexes (N_2Si = *fac*-bis(pyridine-2-iloxy) methylsilyl or *fac*-bis(4-methylpyridine-2-iloxy)methylsilyl) are effective catalysts for the solvent-free selective reduction of CO_2 to silyl-formates [3], the hydrolysis of hydrosilanes to afford the corresponding silanol and hydrogen [4], the synthesis of silylamines by dehydrogenative silylation of secondary amines [5], the synthesis of silylesters by dehydrogenative silylation of carboxylic acids [6], the synthesis of silylphosphanecarboxylates by insertion of CO_2 into the P–Si bond of silylphosphanes [7] and the synthesis of silylcarbamates by insertion of CO_2 into the N–Si bond of silylamines [5]. In addition, rhodium-(*fac*-κ^3-N_2Si) (N_2Si = *fac*-bis(pyridine-2-iloxy)methylsilyl) species catalyzes the formation of silylenolethers by dehydrogenative silylation of acetophenone derivatives [8].

Examples of hydrosilylation catalysts based on iridium complexes with monoanionic bidentate NSi ligands have also been reported. Thus, Ir-(κ^2-NSi^{tBu}) (NSi^{tBu} = (4-methylpyridine-2-iloxy) ditertbutylsilyl) species are effective catalysts for the selective reduction of formamides to *O*-silylated hemiaminals or to amines [9]. Moreover, $Ir(\kappa^2\text{-}NSi^{Me})_2$ (NSi^{Me} = (4-methylpyridine-2-iloxy) dimethylsilyl) complexes are effective catalyst precursors for the selective reduction of CO_2 to silylformate or methoxysilane [10]. Herein, the synthesis and characterization of Rh-(κ^2-NSi^{Me})$_2$ species together with the study of their potential as catalysts for the reaction of secondary amines with CO_2 and hydrosilanes is

* Corresponding author.
E-mail address: paco@unizar.es (F.J. Fernández-Alvarez).

https://doi.org/10.1016/j.jorganchem.2019.06.010
0022-328X/

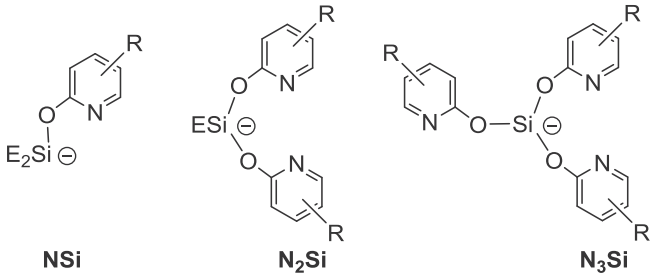

Fig. 1. Examples of monoanionic pyridine-2-iloxy-silyl based ligands (E and R alkyl or aryl groups).

described. The outcomes of these studies revealed that Rh-(κ^2-NSi^{Me})$_2$ species promoted the selective formation of silylcarbamates from the reaction of aliphatic secondary amines with CO_2 and hydrosilanes.

2. Results and discussion

2.1. Synthesis and characterization of the rhodium catalyst precursors

The reaction of two equivalents of the freshly prepared functionalized silane NSi^{Me}–H, (4-methylpyridine-2-yloxy)dimethylsilane, (**1**) [10] with half equivalent of [Rh(μ-Cl)(coe)$_2$]$_2$ (coe = *cis*-cyclooctene) in toluene quantitatively gives the rhodium(III) species [Rh(Cl)(κ^2-NSi^{Me})$_2$] (**2**) (NSi^{Me} = 4-methylpyridine-2-iloxy) dimethylsilyl) (Scheme 1). ^{1}H NMR studies of this reaction showed the presence of free coe and the formation of cyclooctane (coa) along with **2**.

Species **2** reacts with one equivalent of silver trifluoroacetate in CH_2Cl_2 to afford the compound [Rh(CF_3CO_2)(κ^2-NSi^{Me})$_2$] (**3**), which has been isolated as a white solid in 73% yield (Scheme 1). Complexes **2** and **3** have been fully characterized by elemental analysis, ^{1}H, ^{13}C and ^{29}Si NMR spectroscopy and in the case of **3** by X-ray diffraction methods (Fig. 2).

The rhodium atom in complex **3** exhibits a distorted octahedral geometry, with the oxygen atoms of the carboxylate ligand and the silicon atoms in the equatorial plane, and apical positions fulfilled by nitrogen atoms. The rhodium-silicon bond lengths in **3** are in the range 2.2277(8)-2.2388(10) Å. The (κ^2-O) coordination of the carboxylate ligand to the metal is characterized by two long but similar Rh–O bond lengths (around 2.4 Å) and *trans* Si–Rh–O angles close to 160°. The pyridinic rings around the metallic centers in **3** are *trans* disposed one to each other, with similar Rh–N bond

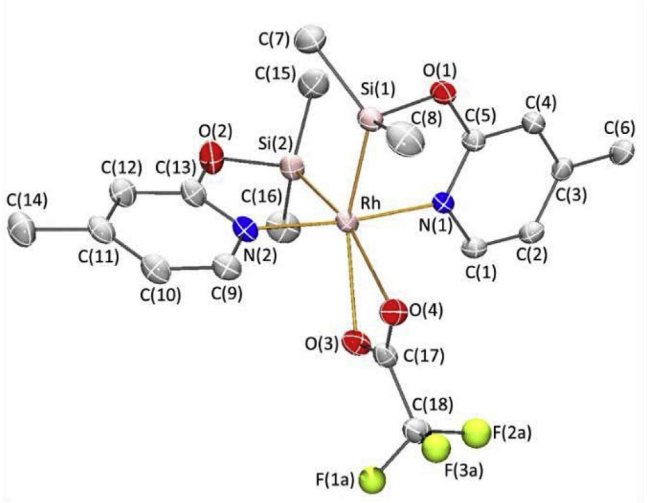

Fig. 2. Molecular structure of complex **3**. Hydrogen atoms have been omitted for clarity. Selected bond lengths (Å) and angles (°): Rh–Si(1), 2.2277(8); Rh–Si(2), 2.2388(10); Rh–O(3), 2.414(2); Rh–O(4), 2.391(2); Rh–N(1), 2.062(3); Rh–N(2), 2.056(3); Si(1)-Rh-Si(2), 91.47(3); Si(1)-Rh-O(3), 158.19(6); Si(1)-Rh-O(4), 104.21(6); Si(1)-Rh-N(1), 81.82(7); Si(1)-Rh-N(2), 93.56(7); Si(2)-Rh-O(3), 109.59(6); Si(2)-Rh-O(4), 163.86(6); Si(2)-Rh-N(1), 93.51(8); Si(2)-Rh-N(2), 81.88(8); O(3)-Rh-O(4), 55.29(7); O(3)-Rh-N(1), 91.03(9); O(3)-Rh-N(2), 94.93(9); O(4)-Rh-N(1), 92.47(9); O(4)-Rh-N(2), 93.21(10); N(1)-Rh-N(2), 173.42(10).

lengths 2.056(3) and 2.062(3) Å. The N–Rh–N arrangement is deviated from the ideal value of 180° (N(1)-Ir(1)-N(2), 173.42(10)°), which could be related to the chelating bonding of NSi^{Me} ligands which leads to the formation of two Ir–Si–*O*–C–N metallacycles, with ring puckering parameters typical of $^2T_1$ and $^2T_1$ with a small contribution of ^2E conformations, respectively [11].

The mononuclear structure proposed in Scheme 1 for complex **2** was corroborated by means of ^{1}H-DOSY NMR spectroscopy [12]. The resonances of the aromatic protons of the NSi^{Me} ligand in CD_2Cl_2 were used for the determination of the diffusion coefficients (D) of complexes **2** and **3** at 300 K. The D value measured for **2** in CD_2Cl_2, 1.163×10^{-9} m^2 s^{-1}, compares well with the D value obtained for **3** under the same conditions, 1.186×10^{-9} m^2 s^{-1}. Therefore, assuming the mononuclear structure found for **3** (Fig. 2), it is reasonable to propose that **2** also possesses a mononuclear structure in solution. In addition, ^{1}H and ^{13}C NMR spectra of complexes **2** and **3** also support the structure proposed for these species. ^{29}Si{^{1}H} NMR spectra show a doublet resonance at δ 85.7 ppm ($^1J_{Rh\text{-}Si}$ = 36.6 Hz) and δ 86.2 ppm ($^1J_{Rh\text{-}Si}$ = 39.3 Hz), respectively, which agrees with the equivalence of the two silicon atoms in both complexes.

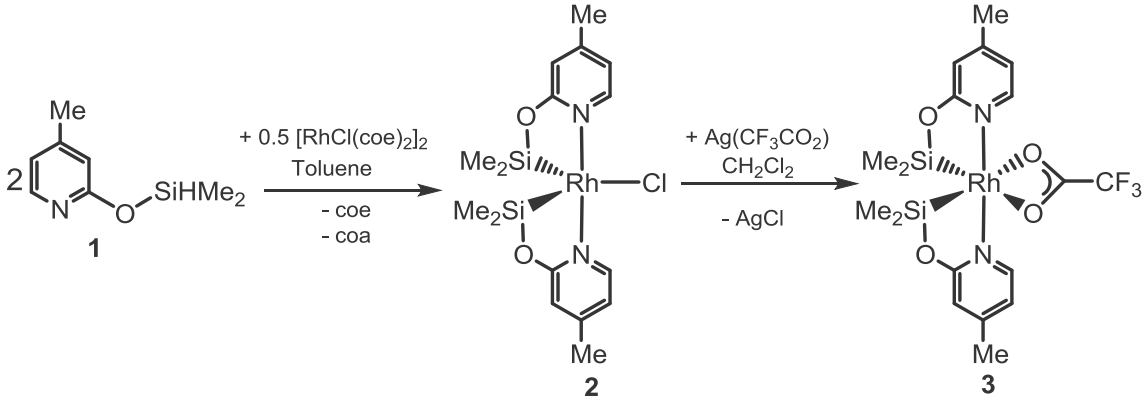

Scheme 1. Synthesis of the rhodium complexes **2** and **3**.

2.2. 3-Catalyzed reaction of secondary amines with hydrosilanes

The development of catalytic methodologies that allow the utilization of CO_2 as C1 raw material for organic synthesis is of great interest [13]. The reaction of amines with CO_2 and hydrosilanes has proven to be an effective methodology for obtaining formamides, methylamines, aminals and/or carbamates [14]. Thus, in presence of a catalyst, secondary and/or primary amines usually react with CO_2 and hydrosilanes to yield formamides. Furthermore, some catalysts can reduce the formamide to the corresponding methylamine (Scheme 2) [14].

In recent years, it has been demonstrated that silylcarbamates could also be obtained from the catalytic reaction of amines with CO_2 and hydrosilanes. The formation of silylcarbamates as minor by-products of the transition metal catalyzed formylation of secondary amines with CO_2 and hydrosilanes was first observed by García et al., in 2013 [15]. Few years later, we found that using the iridium complex [Ir(H)(CF_3SO_3)(NSiN)(coe)] (NSiN = *fac*-bis-(pyridine-2-yloxy)methylsilyl; *coe* = *cis*-cyclooctene) as catalyst (1.0 mol %), it was possible to selective and quantitatively prepare the corresponding silylcarbamate from the reaction of aliphatic secondary amines with CO_2 (3 bar) and one equivalent of $HSiMe(OSiMe_3)_2$ under solvent-free conditions [5]. Examples of heterogeneous catalytic systems based on 10% wt Pd on dry matrix carbon have also proven to be effective for the dehydrogenative formation of silyl carbamates from amines, CO_2 and hydrosilanes [16].

In this context, it has been found that complexes **2** and **3** (1.0 mol%) catalyze the selective reaction of pyrrolidine with CO_2 and $HSiMe_2Ph$ to give the corresponding silylcarbamate *c*-(C_4H_8)NCO_2SiMe_2Ph (**4a**). The ancillary ligand plays a role on the catalytic activity. Thus, complex **3** with a trifluoroacetate ligand allows the conversion of 94% of the starting silane after 6 h, while using **2** around 80% of conversion was obtained in the same time.

The above described outcomes aimed us to explore the performance of the catalytic system based on **3**. The activity of the **3**-catalyzed reaction of pyrrolidine with CO_2 and hydrosilanes depends on the nature of the silicon compound. In all the cases, the reactions were selective to the formation of the corresponding silylcarbamate *c*-(C_4H_8)NCO_2SiR_3 (SiR_3 = $SiMe_2Ph$, **4a**; $SiMePh_2$, **5**; $SiEt_3$, **6**; $SiMe(OSiMe_3)_2$, **7**) (Scheme 3). $HSiMe_2Ph$ is more reactive than $HSiMePh_2$ and $HSiEt_3$, and using $HSiMe(OSiMe_3)_2$ only 12% of the corresponding silylcarbamate **7** was observed after 24 h (Fig. 3). This reactivity trend could be explained considering the lower hindrance around the Si–H bond in $HSiMe_2Ph$ in comparison with the other silicon derivatives studied.

^{1}H NMR studies of the reaction of pyrrolidine with CO_2 (3 bar) and $HSiMe_2Ph$ in C_6D_6 at 323 K in presence of 0.5, 1.0 and 5.0 mol% of **3** evidenced that the catalyst loading moderately influences on the catalytic activity (Fig. S39). In addition, it has been found that the nature of the amine strongly influences the catalytic activity, where the best results were obtained for cyclic secondary amines such as pyrrolidine and piperidine, while the reactions with *N,N*-diisopropylamine bearing a hindered N–H bond were slower (Table 1 and Fig. 4). In addition, no reaction was observed with N-methylaniline.

The silylcarbamates **4a-e**, **5** and **6** were characterized by means of ^{1}H, ^{13}C and ^{29}Si NMR spectroscopy (see experimental and supporting). Compound **7** was characterized by comparison with the reported data [5]. The most noticeable resonances in their ^{13}C {^{1}H} NMR spectra were those corresponding to the carboxylic carbon atom that appears around δ 154 ppm, which agrees with the reported data for analogous compounds [5].

In the absence of complexes **2** and **3**, C_6D_6 solutions of pyrrolidine and $HSiMe_2Ph$ react with CO_2 (3 bar) to quantitatively give a mixture of the corresponding carbamic acid and $HSiMe_2Ph$. This mixture slowly evolves at 323 K to produce the corresponding silylcarbamate and traces of formamide. Thus, after 60 h a 36% of conversion of the carbamic acid into silylcarbamate (30%) and formamide (6%) is observed. These outcomes prove that species **2** and **3** play a relevant role on the above-mentioned catalytic process.

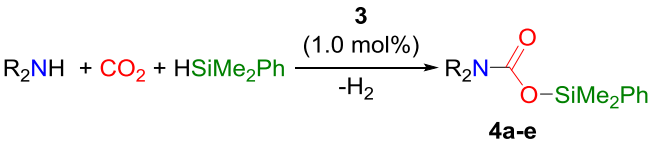

Scheme 3. Preparation of silylcarbamates from the **3**-catalyzed (1.0 mol%) reaction of secondary amines with CO_2 (3 bar) and $HSiMe_2Ph$ in C_6D_6 at 323 K. (R_2 = *c*-(C_4H_8), **4a**; *c*-(C_4H_8O), **4b**; *c*-(C_5H_{10}), **4c**; Et_2, **4d**; $^iPr_2$, **4e**).

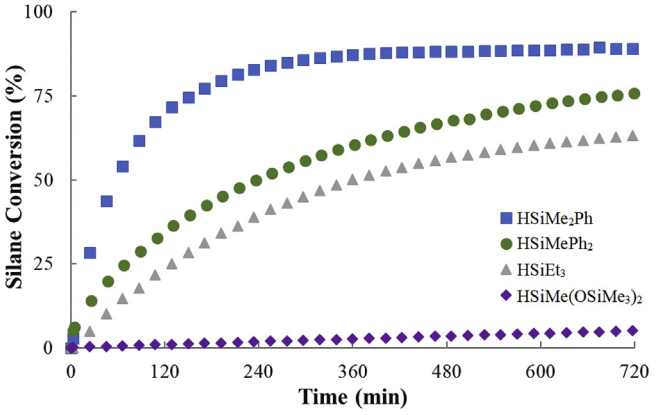

Fig. 3. Representation of hydrosilane conversion (mol %) to *c*-(C_4H_8)NCO_2SiR_3 (SiR_3 = $SiMe_2Ph$, **4a**; $SiMePh_2$, **5**; $SiEt_3$, **6**; $SiMe(OSiMe_3)_2$, **7**) vs time for the **3**-catalyzed (1.0 mol%) reaction of pyrrolidine with CO_2 (3 bar) and the corresponding silane at 323 K in C_6D_6.

Table 1
Selectivity to silylcarbamate from the **3**-catalyzed (1.0 mol%) reaction of secondary amines with CO_2 (3 bar) and $HSiMe_2Ph$ in C_6D_6 at 323 K.

Amine	Carbamate; (%)[a]	Conversion, %[b]	Formamide, %[a]
Pyrrolidine	**4a**; (99)	94	1
Morpholine	**4b**; (96)	78	3
Piperidine	**4c**; (97)	80	4
N,N-diethylamine	**4d**; (97)	92	3
N,N-diisopropylamine	**4e**; (100)	36	–

[a] mol% base on ^{1}H NMR integration; [b] mol% of the starting amine consumed after 14 h of reaction.

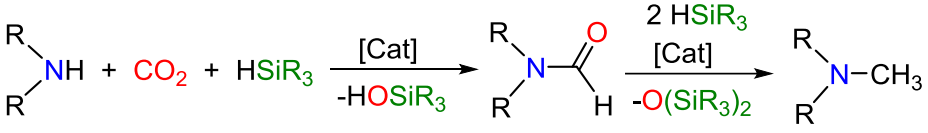

Scheme 2. Catalytic formylation of secondary aliphatic amines (R_2NH) with CO_2 and hydrosilanes.

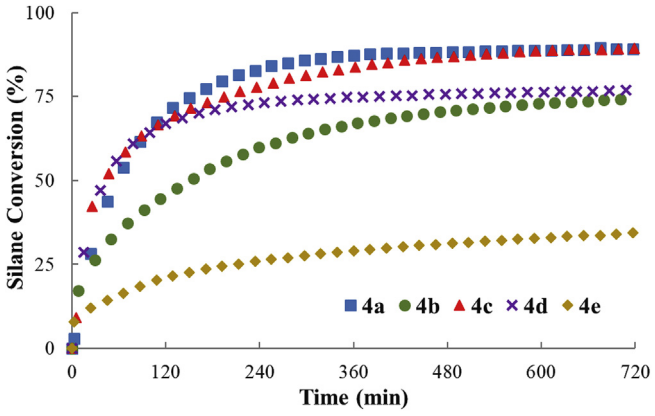

Fig. 4. Representation of $HSiMe_2Ph$ conversion (mol %) to $R_2NCO_2SiMe_2Ph$ (R_2 = *c*-(C_4H_8), **4a**; *c*-(C_4H_8O), **4b**; *c*-(C_5H_{10}), **4c**; Et_2, **4d**; $^iPr_2$, **4e**) vs time for the **3**-catalyzed (1.0 mol%) reaction of secondary amines with CO_2 (3 bar) and $HSiMe_2Ph$ at 323 K in C_6D_6.

Two different reaction pathways have been proposed to explain the catalytic formation of silylcarbamates from the reaction of amines with CO_2 and hydrosilanes (Scheme 4). The first one consists in the insertion of a CO_2 molecule into the Si–N bond of an *in situ* generated silylamine (Scheme 4, *path a*) [5,17–19]. This path requires a previous step consisting in a dehydrogenative silylation of the amine [20,21]. The second possibility is the catalytic dehydrogenative silylation of the corresponding carbamic acid (Scheme 4, *path b*).

It has been demonstrated that, differently to that observed for Ir–N_2Si based catalysts [5], in absence of CO_2, solutions of pyrrolidine and $HSiMe_2Ph$ in presence of catalytic amounts of **3** (1.0 mol %) are stable over time. Indeed, no reaction was observed after 6 h at 343 K. Analogous behavior was observed for piperidine and morpholine. Therefore, under the studied conditions complex **3** is not an active catalyst for the dehydrogenative silylation of secondary amines. Therefore, it is reasonable to discard *path a* of Scheme 4 for explaining the formation of silylcarbamates.

It is worth mentioning that under the reaction conditions, 3 bar of CO_2, the equilibrium between the amine and the corresponding carbamic acid [22] is shifted towards the latter (Fig. 5). This suggest that formation of the silylcarbamate could be consequence of the **3**-catalyzed dehydrogenative silylation of the corresponding carbamic acid according to *path b* in Scheme 4.

In agreement with that possibility, it has been proven that, similarly to other group 9 metal complexes [6], species **3** catalyzes the dehydrogenative silylation of formic acid to afford the silylformate HCO_2SiMe_2Ph (**8**). Thus, the **3**-catalyzed (1.0 mol%) reaction of formic acid with one equivalent of $HSiMe_2Ph$ quantitatively affords

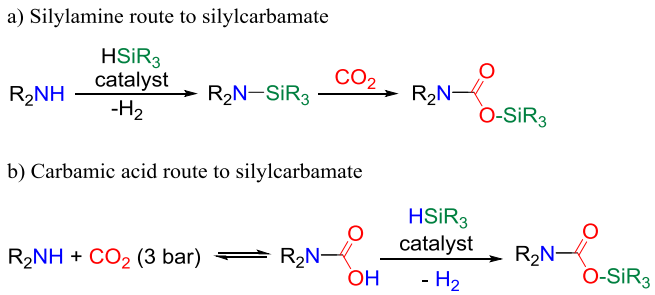

Scheme 4. Possible reaction paths for the catalytic formation of silylcarbamates from aliphatic secondary amines (R_2NH), CO_2 and hydrosilanes.

8 and H_2 (Scheme 5). The silylformate **8** has been characterized by comparison of its ^1H NMR spectra with reported data [3a].

Table 1 illustrates that formamides were obtained as minor side products of these reactions in around 1–4% yield. The obtention of formamides from the catalytic reaction of secondary amines with CO_2 using hydrosilanes as reductants, has been commonly explained because of the reaction of the *in situ* produced silylformates, by CO_2 hydrosilylation, with the corresponding amine [13], or by the catalytic reaction of silylcarbamates with hydrosilanes to yield formamides and the corresponding siloxane [23] (Scheme 6).

In this regard, it should be mentioned that the ^1H NMR studies of the **3**-catalyzed reaction of CO_2 (3 bar) with $HSiMe_2Ph$ in C_6D_6 at 323 K revealed that after 24 h of reaction only traces of the corresponding silylformate **8** were formed. Moreover, the **3**-catalyzed reaction of pyrrolidine with CO_2 (3 bar) in presence of four equivalents of $HSiMe_2Ph$ quantitatively affords the silylcarbamate **4a**, which did not react with the excess of $HSiMe_2Ph$ present in the reaction mixture, even after 24 h at 323 K. Therefore, the low concentration of formamide observed along the above described reactions (Table 1) could be consequence of the poor activity of **3** as CO_2 and/or silylcarbamates hydrosilylation catalyst.

3. Experimental

3.1. General information

All manipulations were performed with rigorous exclusion of air at an argon/vacuum manifold using standard Schlenk-tube techniques or in MBraun glovebox when necessary. Solvents were dried and distilled under argon by standard procedures prior to use or purified by a Solvent Purification System (Innovative Technologies). NMR spectra were obtained on a Bruker ARX-300, Bruker AV-300 MHz or Varian Gemini 2000. Chemical shifts (δ), reported in ppm, were referenced to the residual peaks of deuterated solvents. Compound **1** was prepared according to the method reported in the literature [10]. Carbon dioxide (99.99% purity) was purchased from commercial sources.

3.2. Synthesis of [Rh(Cl)(κ^2-NSi^{Me})$_2$] (**2**)

A toluene solution (5 mL) of compound **1** (0.300 g, 1.800 mmol) was slowly added to a suspension of [Rh(μ-Cl)(coe)$_2$]$_2$ (0.760 g, 0.848 mmol) in toluene (10 mL) and the resulting mixture was stirred at room temperature for 2 h. The solvent was removed in vacuo and the residue washed with pentane cooled at 273 K (3 × 10 mL) to afford a pale brown solid. Yield: 0.320 g (76%). Anal. Calcd. For $C_{16}H_{24}ClRhN_2O_2Si_2$: C, 40.81; H, 5.14; N, 5.95. Found: C, 40.84; H, 5.15; N, 6.09. ^1H NMR plus HSQC ^1H–^{13}C (300 MHz, 298 K, CD_2Cl_2): δ 8.58 (d, $^3J_{H\text{-}H}$ = 6.1 Hz, 2H, py-*6*), 6.67 (m, 2H, py-*3*), 6.59 (dd, $^3J_{H\text{-}H}$ = 6.1 Hz, $^5J_{H\text{-}H}$ = 1.8 Hz, 2H, py-*5*), 2.30 (s, 6H, *CH*$_3$-py), 0.65 (s, 6H, SiMe), 0.40 (s, 6H, SiMe). $^{13}C\{^1H\}$ APT plus HSQC ^1H–^{13}C (75 MHz, 298 K, CD_2Cl_2): δ 166.8 (s, *C*$_2$-py), 152.8 (s, *C*$_4$-py), 150.3 (s, *C*$_6$-py), 118.4 (s, *C*$_5$-py), 112.0 (s, *C*$_3$-py), 21.3 (s, *CH*$_3$-py), 6.8 (s, SiMe), 3.8 (d, $^2J_{Rh\text{-}H}$ = 4.0 Hz, SiMe). $^{29}Si\{^1H\}$ NMR (HMBC ^1H–^{29}Si, 298 K, CD_2Cl_2): δ 85.7 (d, $^1J_{Rh\text{-}Si}$ = 36.6 Hz). High Resolution Mass Spectrometry (ESI$^+$): calc. *m/z* = 435.0432; found *m/z* = 434.9765 ($M^+ - Cl$).

3.3. Synthesis of [Rh(CF_3CO_2)(κ^2-NSi^{Me})$_2$] (**3**)

CH_2Cl_2 (15 mL) was added to a light-protected Schlenk tube containing a mixture of complex **2** (0.300 g, 0.320 mmol) and silver trifluoroacetate (0.150 g, 0.680 mmol). The resulting suspension was stirred at room temperature for 4 h and filtered out through Celite. The solvent was removed in vacuo and the residue washed

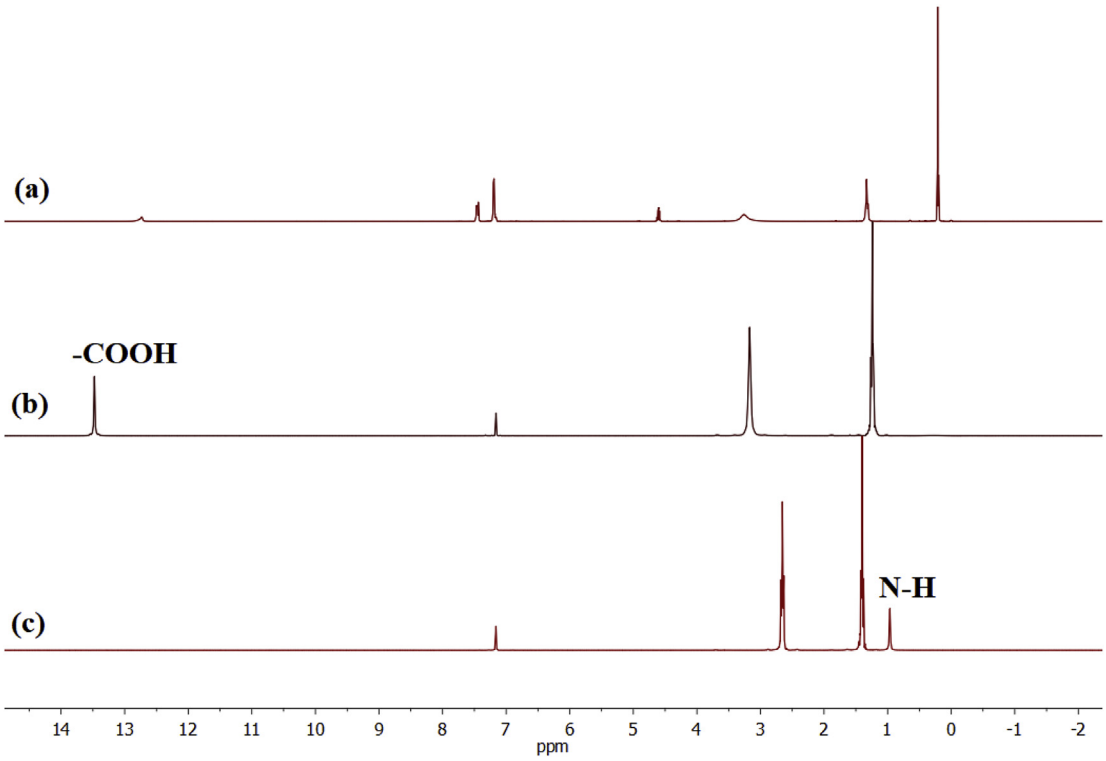

Fig. 5. (a) ^{1}H NMR spectrum of the **3** catalyzed reaction of pyrrolidine, CO_2 (3 bar) and $HSiMe_2Ph$ before heating. (b) ^{1}H NMR spectrum of pyrrolidine under atmosphere of CO_2 (3 bar) in C_6D_6 at 298 K. (c) ^{1}H NMR spectrum of pyrrolidine in C_6D_6 at 298 K.

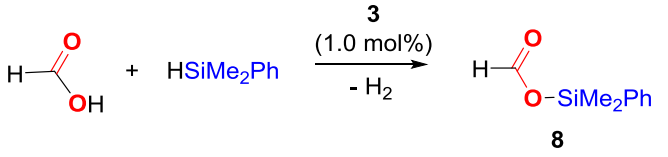

Scheme 5. Dehydrogenative silylation of formic acid with $HSiMe_2Ph$ catalyzed by **3** (1.0 mol%).

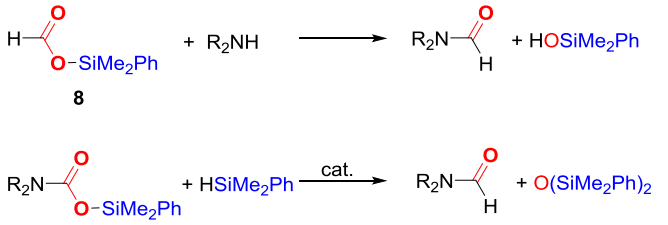

Scheme 6. Possible pathways to explain the formation of formamides as side reaction products.

with cold pentane (198 K, 3 × 10 mL) to afford a white solid. Yield 0.255 g (73%). Anal. Calcd. For $C_{18}H_{24}F_3RhN_2O_4Si_2$: C, 39.42; H, 4.41; N, 5.11. Found: C, 39.32; H, 4.25; N, 4.98. ^{1}H NMR plus HSQC ^{1}H–^{13}C (300 MHz, 298 K, CD_2Cl_2): δ 7.96 (d, $^{3}J_{H\text{-}H} = 6.0$ Hz, 2H, py-*6*), 6.69 (s, 2H, py-*3*), 6.67 (d, $^{3}J_{H\text{-}H} = 6.0$ Hz, 2H, py-*5*), 2.30 (s, 6H, CH_3-py), 0.61 (s, 6H, SiMe), 0.41 (s, 6H, SiMe). ^{13}C{^{1}H} NMR APT plus HSQC ^{1}H–^{13}C (75 MHz, 298 K, CD_2Cl_2): δ 166.7 (s, C_2-py), 153.1 (s, C_4-py), 147.7 (s, C_6-py), 118.9 (s, C_5-py), 112.4 (s, C_3-py), 21.3 (s, CH_3-py), 4.6 (s, SiMe), 3.2 (d, $^{2}J_{Rh\text{-}H} = 4.4$ Hz, SiMe). ^{19}F{^{1}H} NMR (282 MHz, 298 K, CD_2Cl_2): δ −75.6 (CF_3CO_2). ^{29}Si NMR (HMBC ^{1}H–^{29}Si, 298 K, CD_2Cl_2): δ 86.2 (d, $^{1}J_{Rh\text{-}Si} = 39.3$ Hz). High Resolution Mass Spectrometry (ESI^{+}): calc. $m/z = 435.0432$; found $m/z = 435.0423$ (M^{+}-CF_3CO_2).

3.4. 3-Catalyzed (1.0 mol%) reactions

A Young cap NMR tube was filled with the catalyst precursor **3** (2.00 mg, 3.64 μmol), $HSiMe_2Ph$ (0.401 mmol, 61.5 μL), amine (0.364 mmol) and 0.5 mL of C_6D_6. Argon was removed under reduced pressure after freezing the solution, and the tube was then pressurized with CO_2 (3 bar) and heated to 323 K. The same procedure was followed for the reactions of pyrrolidine with other silanes ($HSiMePh_2$, 80.0 μL; $HSiEt_3$, 64 μL; $HSiMe(OSiMe_3)_2$, 109.0 μL).

3.5. 3-Catalyzed (1.0 mol%) dehydrogenative silylation of formic acid

A Young cap NMR tube was filled with the catalyst precursor **3** (2.00 mg, 3.64 μmol), $HSiMe_2Ph$ (0.401 mmol, 61.5 μL), formic acid (0.364 mmol, 13.7 μL) and 0.5 mL of C_6D_6. The mixture was then heated at 323 K and monitored by ^{1}H NMR spectroscopy.

3.6. Selected NMR data of the catalytic products

3.6.1. c-(C_4H_8)N–C(O)O$SiMe_2Ph$ (**4a**)

^{1}H NMR (300 MHz, C_6D_6, 298 K): δ 7.78–7.75 (m, 2H, Ph), 7.28–7.20 (m, 3H, Ph), 3.23–3.05 (m, 4H, N–CH_2), 1.24–1.20 (m, 4H, –CH_2-), 0.66 (s, 6H, $SiCH_3$). ^{13}C NMR APT (75 MHz, C_6D_6): δ 153.6 (s, CO_2Si), 137.4 (s, C_{ipso}-Ph), 134.1 (s, Ph), 130.1 (s, Ph), 128.2 (s, Ph), 46.5 (s, N–CH_2), 46.1 (s, N–CH_2), 25.7 (s, CH_2), 25.1 (s, CH_2), −0.8 (s, $SiCH_3$). ^{29}Si{^{1}H} NMR (HMBC ^{29}Si–^{1}H, 298 K): δ 9.8 (s, $SiCH_3$).

3.6.2. c-(C_4H_8O)N–C(O)O$SiMe_2Ph$ (**4b**)

^{1}H NMR (300 MHz, C_6D_6, 298 K): δ 7.71–7.68 (m, 2H, Ph),

7.25–7.21 (m, 3H, Ph), 3.23–3.13 (m, 8H, $-CH_2$-), 0.61 (s, 6H, $SiCH_3$). ^{13}C NMR APT (75 MHz, C_6D_6): δ 154.0 (s, CO_2Si), 136.8 (s, C_{ipso}-Ph), 134.1 (s, Ph), 130.3 (s, Ph), 128.2 (s, Ph), 66.4 (s, O–CH_2), 45.3 (s, N–CH_2), 44.0 (s, N–CH_2), −1.1 (s, $SiCH_3$). $^{29}Si\{^1H\}$ NMR (HMBC $^{29}Si-^1H$, 298 K): δ 10.9 (s, $SiCH_3$).

3.6.3. c-(C_5H_{10})N–C(O)OSiMe$_2$Ph (**4c**)

^1H NMR (300 MHz, C_6D_6, 298 K): δ 7.74–7.71 (m, 2H, Ph), 7.24–7.21 (m, 3H, Ph), 3.28 (br s, 4H, N–CH_2), 1.13 (br s, 6H, $-CH_2$-), 0.63 (s, 6H, $SiCH_3$). ^{13}C NMR APT (75 MHz, C_6D_6): δ 154.1 (s, CO_2Si), 137.3 (s, C_{ipso}-Ph), 134.1 (s, Ph), 130.3 (s, Ph), 128.2 (s, Ph), 45.8, 44.7 (s, N–CH_2), 26.1, 25.7 (s, -CH_2-), 24.4 (s, -CH_2-), −0.9 (s, $SiCH_3$). $^{29}Si\{^1H\}$ NMR (HMBC $^{29}Si-^1H$, 298 K): δ 10.0 (s, $SiCH_3$).

3.6.4. Et$_2$N–C(O)OSiMe$_2$Ph (**4d**)

^1H NMR (300 MHz, C_6D_6, 298 K): δ 7.72–7.69 (m, 2H, Ph), 7.25–7.19 (m, 3H, Ph), 3.11–2.98 (m, 4H, N–CH_2), 0.89 (br, 6H, CH_3), 0.61 (s, $SiCH_3$). ^{13}C NMR APT (75 MHz, C_6D_6): δ 154.6 (s, CO_2Si), 137.4 (s, C_{ipso}-Ph), 134.0 (s, Ph), 130.1 (s, Ph), 128.2 (s, Ph), 42.0, 41.7 (s, N–CH_2), 14.3, 13.5 (s, CH_3), −0.9 (s, $SiCH_3$). $^{29}Si\{^1H\}$ NMR (HMBC $^{29}Si-^1H$, 298 K): δ 10.1 (s, $SiCH_3$).

3.6.5. ^{i}Pr$_2$N–C(O)OSiMe$_2$Ph (**4e**)

^1H NMR (300 MHz, C_6D_6, 298 K): δ 7.74–7.71 (m, 2H, Ph), 7.23–7.19 (m, 3H, Ph), 3.90–3.56 (m, 2H, N–CH), 1.04 (d, $J = 6.8$ Hz, 12H, CH_3), 0.62 (s, $SiCH_3$). ^{13}C NMR APT (75 MHz, C_6D_6): δ 154.2 (s, CO_2Si), 137.5 (s, C_{ipso}-Ph), 134.1 (s, Ph), 130.0 (s, Ph), 128.1 (s, Ph), 46.2 (s, N–CH), 21.5, 20.5 (br s, CH_3), −0.8 (s, $SiCH_3$). $^{29}Si\{^1H\}$ NMR (HMBC $^{29}Si-^1H$, 298 K): δ 9.4 (s, $SiCH_3$).

3.6.6. c-(C_4H_8)N–C(O)OSiMePh$_2$ (**5**)

^1H NMR (300 MHz, C_6D_6, 298 K): δ 7.84–7.82 (m, 4H, Ph), 7.25–7.24 (m, 6H, Ph), 3.29 (br s, 4H, N–CH_2), 1.36 (m, 4H, CH_2), 0.99 (s, 3H, $SiCH_3$). ^{13}C NMR APT (75 MHz, C_6D_6): δ 153.2 (s, CO_2Si), 137.9 (s, C_{ipso}-Ph), 135.1 (s, Ph), 130.3 (s, Ph), 128.2 (s, Ph), 46.2 (br s, N–CH_2), 25.4 (br s, CH_2), 25.2 (s, CH_2), −1.7 (s, $SiCH_3$). $^{29}Si\{^1H\}$ NMR (HMBC $^{29}Si-^1H$, 298 K): δ −1.0 (s, $SiCH_3$).

3.6.7. c-(C_4H_8)N–C(O)OSiEt$_3$ (**6**)

^1H NMR (300 MHz, C_6D_6, 298 K): δ 3.23–3.10 (m, 4H, N–CH_2), 1.06 (m, 9H, CH_3), 0.86 (s, 6H, $SiCH_2$). ^{13}C NMR APT (75 MHz, C_6D_6): δ 153.7 (s, CO_2Si), 46.5 (s, N–CH_2), 46.1 (s, N–CH_2), 25.8 (s, CH_2), 25.2 (s, CH_2), 8.4 (s, CH_3), 5.4 (s, $SiCH_2$). $^{29}Si\{^1H\}$ NMR (HMBC $^{29}Si-^1H$, 298 K): δ 22.3 (s, $SiCH_3$).

3.7. Crystal structure determination of complex **3**

X-ray diffraction data were collected at 100(2)K on an automatic Smart APEX Bruker diffractometer with graphite-monochromated Mo Kα radiation (λ = 0.71073 Å) using ω scans with narrow oscillation frames (0.3°). Diffracted intensities were integrated and corrected from absorption effects with SAINT+ [24] and SADABS [25] programs, included in APEX 3 package. The structure was solved by direct methods and refined with SHELXS-2013 [26] and refined with full-matrix least-squares refinement with SHELXL-2018 [27] programs included in WingX package [28].

Crystal Data for **3**: $C_{18}H_{24}F_3N_2O_4RhSi_2$; Mr = 548.48; yellow prism, 0.180 × 0.200 × 0.215 mm; Orthorhombic *Pna21*; a = 20.5601(9) Å, b = 8.1427(4) Å, c = 14.0964(6) Å; V = 2359.94(18) Å^3; $Z = 4$; $\rho_{calcd} = 1.544$ g cm^{-3}; $\mu = 0.874$ cm^{-1}; minimum and maximum transmission factors 0.8164 and 0.8749; $2\theta_{max} = 58.028°$; 43100 reflections collected; 5994 unique reflections ($R_{int} = 0.0212$); number of data/restraints/parameters 5994/1/289; final $GOF = 1.050$; $R_1 = 0.0226$ [5848 reflections, $I > 2\sigma(I)$], w$R2 = 0.0536$ for all data; largest difference peak 0.657 e Å^{-3}.

Hydrogen atoms were included in the model in calculated positions and refined with a riding model. Fluorine atoms have been found to be disordered. They have been included in the model in three sets of positions with 0.42/0.30/0.28(1) occupancy factors and isotropically refined.

CCDC 1906237 contains the supplementary crystallographic data for this paper. The data can be obtained free of charge from The Cambridge Crystallographic Data Centre via www.ccdc.cam.ac.uk/structures.

4. Conclusions

The reaction of (4-methyl-pyridine-2-iloxy)dimethylsilane (NSi^{Me}–H, **1**) with $[RhCl(coe)_2]_2$ gives $[Rh(Cl)(\kappa^2\text{-}NSi^{Me})_2]$ (**2**), which reacts with a stoichiometric amount of $AgCF_3CO_2$ to afford $[Rh(\kappa^2\text{-}CF_3CO_2)(\kappa^2\text{-}NSi^{Me})_2]$ (**3**). Complexes **2** and **3** have been fully characterized by elemental analysis and NMR spectroscopy. In addition, the solid-state structure of **3** has been confirmed by X-ray diffraction studies.

Complex **3** is an effective catalyst for the selective formation of silylcarbamates from the reaction of aliphatic secondary amines with CO_2 and hydrosiloxanes. Moreover, it has been demonstrated that **3** is an active catalyst for dehydrogenative silylation of carboxylic acids. However, under the studied conditions, **3** is a poor catalyst for the hydrosilylation of CO_2 and for the dehydrogenative silylation of amines.

These outcomes allow to conclude that the **3**-catalyzed dehydrogenative silylation of the carbamic acid *in situ* generated by reaction of the corresponding secondary amine with CO_2 is the determining step for explaining the selective formation of silylcarbamates from the **3**-catalyzed reaction of secondary amines with CO_2 and $HSiMe_2Ph$.

Acknowledgements

The financial support from MINECO/FEDER project CTQ2015-67366-P and DGA/FSE project E42_17R is gratefully acknowledged. Dr. P. García-Orduña acknowledges CSIC, European Social Fund and Ministerio de Economía y Competitividad of Spain for a PTA contract. Authors would like to acknowledge the use of Servicio General de Apoyo a la Investigación-SAI, Universidad de Zaragoza.

Appendix A. Supplementary data

Supplementary data to this article can be found online at https://doi.org/10.1016/j.jorganchem.2019.06.010.

References

[1] L. Ehrlich, R. Gericke, E. Brendler, J. Wagler, Inorganics 6 (2018) 119, https://doi.org/10.3390/inorganics6040119.
[2] F.J. Fernández-Alvarez, R. Lalrempuia, L.A. Oro, Coord. Chem. Rev. 350 (2017) 49–60.
[3] (a) A. Julián, J. Guzmán, E.A. Jaseer, F.J. Fernández-Alvarez, R. Royo, V. Polo, P. García-Orduña, F.J. Lahoz, L.A. Oro, Chem. Eur J. 23 (2017) 11898–11907; (b) A. Julián, E.A. Jaseer, K. Garcés, F.J. Fernández-Alvarez, P. García-Orduña, F.J. Lahoz, L.A. Oro, Catal. Sci.Technol. 6 (2016) 4410–4417; (c) R. Lalrempuia, M. Iglesias, V. Polo, P.J. Sanz Miguel, F.J. Fernández-Alvarez, J.J. Pérez-Torrente, L.A. Oro, Angew. Chem. Int. Ed. 51 (2012) 12824–12827.
[4] K. Garcés, F.J. Fernández-Alvarez, V. Polo, R. Lalrempuia, J.J. Pérez-Torrente, L.A. Oro, ChemCatChem 6 (2014) 1691–1697.
[5] A. Julián, V. Polo, E.A. Jaseer, F.J. Fernández-Alvarez, L.A. Oro, ChemCatChem 7 (2015) 3895–3902.
[6] A. Julián, K. Garcés, R. Lalrempuia, E.A. Jaseer, P. García-Orduña, F.J. Fernández-Alvarez, F.J. Lahoz, L.A. Oro, ChemCatChem 10 (2018) 1027–1034.
[7] A. Julián, V. Polo, F.J. Fernández-Alvarez, L.A. Oro, Catal. Sci. Technol. 7 (2017) 1372–1378.
[8] K. Garcés, R. Lalrempuia, V. Polo, F.J. Fernández-Alvarez, P. García-Orduña,

F.J. Lahoz, J.J. Pérez-Torrente, L.A. Oro, Chem. Eur J. 22 (2016) 14717–14729.
[9] J. Guzmán, A.M. Bernal, P. García-Orduña, F.J. Lahoz, L.A. Oro, F.J. Fernández-Alvarez, Dalton Trans. 48 (2019) 4255–4262.
[10] J. Guzmán, P. García-Orduña, V. Polo, F.J. Lahoz, L.A. Oro, F.J. Fernández-Alvarez, Catal. Sci. Technol. 9 (2019) 2858–2867.
[11] D. Cremer, J.A. Pople, J. Am. Chem. Soc. 97 (1975) 1354–1358.
[12] G.A. Morris, Diffusion-ordered spectroscopy, in: R.K. Harris, R.E. Wasylishen (Eds.), Encyclopedia of Magnetic Resonance, Wiley, Chichester, U.K., 2009.
[13] (a) N.A. Tappe, R.M. Reich, V. D'Elia, F.E. Kühn, Dalton Trans. 47 (2018) 13281–13313;
(b) T.P. Senftle, E.A. Carter, Acc. Chem. Res. 50 (2017) 472–475;
(c) X.-B. Lu (Ed.), Carbon Dioxide and Organometallics, Top. Organomet. Chem., vol. 53, Springer International Publishing Switzerland, Heidelberg, 2016;
(d) M. Cokoja, C. Bruckmeier, B. Rieger, W.A. Herrmann, F.E. Kühn, Angew. Chem. Int. Ed. 50 (2011) 8510–8537;
(e) M. Aresta (Ed.), Carbon Dioxide as Chemical Feedstock, Wiley-VCH, Weinheim, 2010;
(f) Q. Yi, W. Li, J. Feng, K. Xie, Chem. Soc. Rev. 44 (2015) 5409–5445.
[14] (For recent reviews see:) (a) F.J. Fernández-Alvarez, L.A. Oro, ChemCatChem 10 (2018) 4783–4796;
(b) R.A. Pramudita, K. Motokura, Green Chem. 20 (2018) 4834–4843;
(c) X. Frogneux, E. Blondiaux, P. Thuéry, T. Cantat, ACS Catal. 5 (2015) 3983–3987;
(d) A. Tlili, E. Blondiaux, X. Frogneux, T. Cantat, Green Chem. 17 (2015) 157–168;
(e) I. Sorribes, K. Junge, M. Beller, Chem. Eur J. 20 (2014) 7878–7883;
(f) Y. Li, X. Fang, K. Junge, M. Beller, Angew. Chem. Int. Ed. 52 (2013) 9568–9571.
[15] L. González-Sebastián, M. Flores-Alamo, J.J. García, Organometallics 32 (2013) 7186–7194.
[16] S. Tanaka, T. Yamamura, S. Nakane, M. Kitamura, Chem. Commun. 51 (2015) 13110–13112.
[17] (a) M. Herbig, U. Böhme, E. Kroke, Inorg. Chim. Acta 473 (2018) 20–28;
(b) K. Kraushaar, C. Wiltzsch, J. Wagler, U. Böhme, A. Schwarzer, G. Roewer, E. Kroke, Organometallics 31 (2012) 4779–4785;
(c) C. Wiltzsch, K. Kraushaar, A. Schwarzer, E. Kroke, Z. Naturforsch 66b (2011) 917–922;
(d) M.J. Fuchter, C.J. Smith, M.W.S. Tsang, A. Boyer, S. Saubern, J.H. Ryan, A.B. Holmes, Chem. Commun. (2008) 2152–2154.
[18] For a recent review see: K. Kraushaar, D. Schmidt, A. Schwarzer, E. Kroke Adv. Inorg. Chem. 66 (2014) 117–162.
[19] M. Xu, A.R. Jupp, M.S.E. Ong, K.I. Burton, S.S. Chitnis, D.W. Stephan, Angew. Chem. Int. Ed. 58 (2019) 5707–5711.
[20] For a recent review on catalytic formation of silicon–heteroatom bonds see: K. Kuciński, G. Hreczycho ChemCatChem 9 (2017) 1868–1885.
[21] (a) M.P. Cibuzar, R. Waterman, Organometalics 37 (2018) 4395–4401;
(b) P. Rios, M. Roselló-Merino, O. Rivada-Wheelaghan, J. Borge, J. López-Serrano, S. Conejero, Chem. Commun. 54 (2018) 619–622;
(c) L.K. Allen, R. García-Rodríguez, D.S. Wright, Dalton Trans. 44 (2015) 12112–12118;
(d) J. Hermeke, H.F.T. Klare, M. Oestreich, Chem. Eur J. 20 (2014) 9250–9254;
(e) C. D.F. Königs, M.F. Müller, N. Aiguabella, H.F.T. Klare, M. Oestreich, Chem. Commun. 49 (2013) 1506–1508;
(f) W. Xie, H. Hu, C. Cui, Angew. Chem. Int. Ed. 51 (2012) 11141–11144;
(g) J.F. Dunne, S.R. Neal, J. Engelkemier, A. Ellern, A.D. Sadow, J. Am. Chem. Soc. 133 (2011) 16782–16785;
(h) D.V. Gutsulyak, S.F. Vyboishchikov, G.I. Nikonov, J. Am. Chem. Soc. 132 (2010) 5950–5951;
(i) F. Buch, S. Harder, Organometallics 26 (2007) 5132–5135;
(j) K. Takaki, K. Komeyama, K. Takehira, Tetrahedron 59 (2003) 10381–10395;
(k) J.X. Wang, A.K. Dash, J.C. Berthet, M. Ephritikhine, M.S. Eisen, J. Organomet. Chem. 610 (2000) 49–57;
(l) J.A. Reichl, D.H. Berry, Adv. Organomet. Chem. 43 (1999) 197–265;
(m) J. He, H.Q. Liu, J.F. Harrod, R. Hynes, Organometallics 13 (1994) 336–343;
(n) H.Q. Liu, J.F. Harrod, Organometallics 11 (1992) 822–827;
(o) H.Q. Liu, J.F. Harrod, Can. J. Chem. 70 (1992) 107–110;
(p) L.H. Sommer, J.D. Citron, J. Org. Chem. 32 (1967) 2470–2472.
[22] M. Aresta, D. Ballivet-Tkatchenko, D. Belli Dell'Amico, M.C. Bonnet, D. Boschi, F. Calderazzo, R. Faure, L. Labella, F. Marchetti, Chem. Commun. (2000) 1099–1100.
[23] H. Lv, Q. Xing, C. Yue, Z. Lie, F. Li, Chem. Commun. 52 (2016) 6545–6548.
[24] SAINT+ in APEX3 V 2017.3, Area Detector Integration Software, Bruker AXS, Madison, WI, 2008.
[25] L. Krause, R. Herbst-Irmer, G.M. Sheldrick, D. Stalke, J. Appl. Crystallogr. 48 (2015) 3–10.
[26] G.M. Sheldrick, Acta Crystallogr. A64 (2008) 112–122.
[27] G.M. Sheldrick, Acta Crystallogr. C71 (2015) 3–8.
[28] L.J. Farrugia, J. Appl. Crystallogr. 45 (2012) 849–854.